iScience

CellPress
OPEN ACCESS

Article

Measurement of trace ^{129}I in natural water with ozone reaction for effective separation of spectral interferences

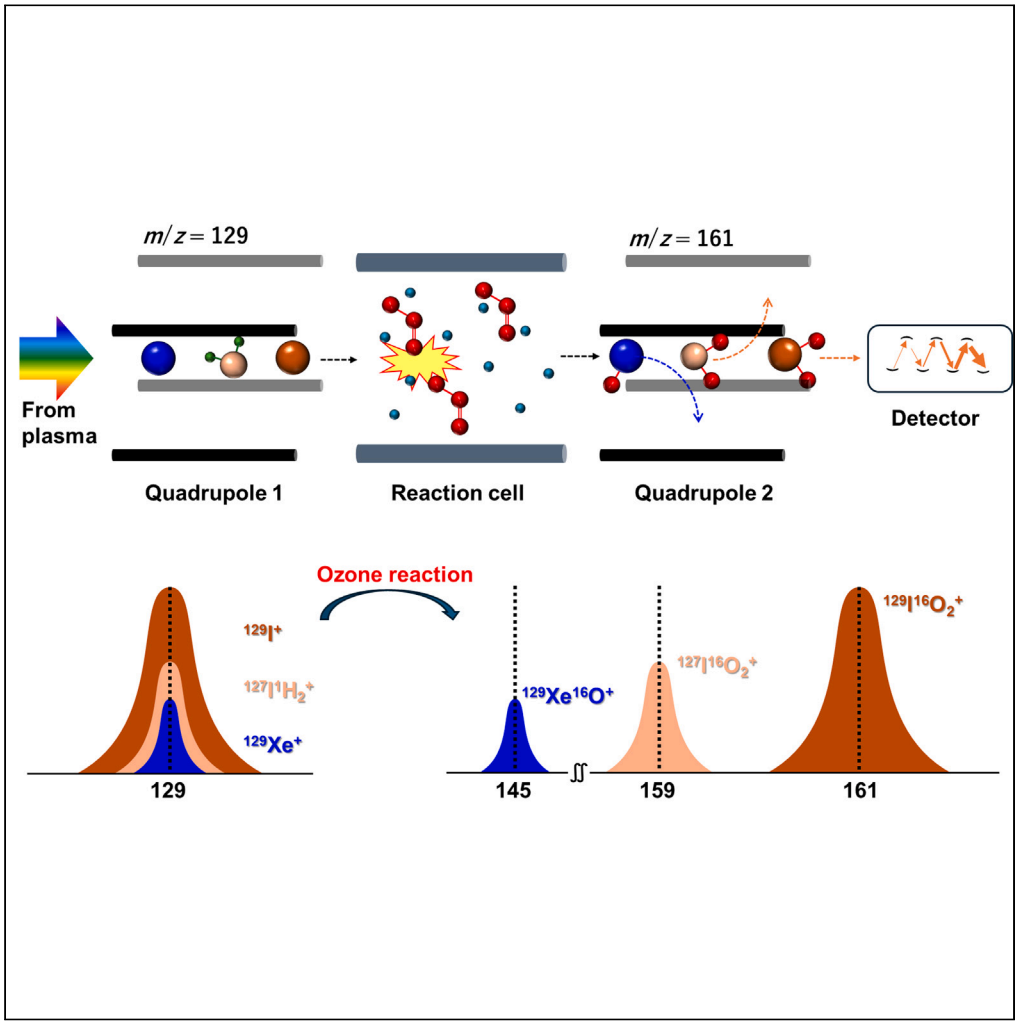

Yanbei Zhu, Daiki Asakawa

yb-zhu@aist.go.jp (Y.Z.)
d.asakawa@aist.go.jp (D.A.)

Highlights

Quantum chemical calculations showed potential merits of O_3 for measuring $^{129}I^+$

On-line generated ozone was used as the reaction gas for measuring of $^{129}I^+$

The detection limit and the BEC of ^{129}I were 0.062 pg/mL and 0.016 pg/mL

The $^{129}I/^{127}I$ ratio in 500 μg/mL natural iodine was observed to be 6.7×10^{-10}

Zhu & Asakawa, iScience 27, 111138
December 20, 2024
https://doi.org/10.1016/j.isci.2024.111138

iScience

CellPress
OPEN ACCESS

Article

Measurement of trace ^{129}I in natural water with ozone reaction for effective separation of spectral interferences

Yanbei Zhu[1,2,*] and Daiki Asakawa[1,*]

SUMMARY

Tandem quadrupole inductively coupled plasma mass spectrometry has the potential capability to measure ^{129}I at extremely low concentration if spectral interferences from ^{129}Xe and $^{127}I^{1}H_2$ can be eliminated effectively. Ozone was introduced as the reaction gas, resulting significantly improved reactions of ($^{129}I^+ \rightarrow {}^{129}I^{16}O^+$) and ($^{129}I^+ \rightarrow {}^{129}I^{16}O_2{}^+$), and permitted the highly sensitive measurement of $^{129}I^+$ as $^{129}I^{16}O^+$ and $^{129}I^{16}O_2{}^+$, helping eliminate spectral interferences related to $^{129}Xe^+$ and $^{127}I^{1}H_2{}^+$. In isotopic ratio ($^{129}I/^{127}I$) analysis by measuring ($^{129}I^+ \rightarrow {}^{129}I^{16}O_2{}^+$)/($^{127}I^+ \rightarrow {}^{127}I^{16}O_2{}^+$), a blank ratio of 6.7×10^{-10} can be realized for a solution of 500 μg/mL natural iodine, improved by one order of magnitude than the best performance previous reported. This technique contributes to the measurement of trace level ^{129}I, a radionuclide of iodine attracting attentions as a geochemical tracer related to the development and civilian use of nuclear energy as well as a regulated radionuclide with guidance levels in drinking water established by the World Health Organization.

INTRODUCTION

Iodine-129 (^{129}I, half-life 15.7 Ma) is one of the long-lived cosmogenic radionuclides.[1] Naturally occurring iodine has an isotopic ratio of $^{129}I/^{127}I$ at 10^{-13} order or lower. This measurement usually requires accelerator mass spectrometry (AMS). This type of low isotopic ratio of $^{129}I/^{127}I$ can indicate old materials whose ^{129}I has decayed. The natural isotopic ratio of $^{129}I/^{127}I$ in marine sediments exhibits steadier value of 1.5×10^{-12},[2] while this ratio in terrestrial sediments is in the larger range of 1.5×10^{-12} to 3.0×10^{-11}.[3–5] Measurement of ^{127}I via inductively coupled plasma mass spectrometry (ICP-MS) is often conducted along with isotopic ratio analysis of $^{129}I/^{127}I$ via AMS to determine the concentration of ^{129}I in the sample.[6–16]

Meanwhile, anthropogenic ^{129}I is gathering attention as a geochemical tracer due to its release associated with nuclear weapons testing, nuclear accidents, nuclear reprocessing facilities, and nuclear power plants.[17] The isotopic ratios of $^{129}I/^{127}I$ in the environment reached in the range from 10^{-10} to 10^{-4} and some of the measurement can be realized with ICP-MS.[18] Determination of ^{129}I by ICP-MS have been continuously examined by researchers around the world since early 1990s.[19–43] Spectral interferences (especially due to ^{129}Xe and $^{127}I^{1}H_2$) are always an obstacle to the determination of ^{129}I at extremely low concentrations. The instrumental detection limit for ^{129}I was reported under 1.0 pg/mL (equivalent to 6.5 mBq/L) with latest ICP-MS instruments.[26,30,31,42] This limit was significantly improved when compared to those obtained in 1990s at tens of pg/mL.[24,41,43] The introduction of reaction cell technique aids in improving the detection of ^{129}I by ICP-MS, where oxygen is often used as the cell gas.[20,21,23,25,26,28–30,32–35,37–40,42] In most cases, ^{129}I is measured as $^{129}I^+$ by ICP-MS with spectral interferences suppressed by reactions with cell gas, along with mathematic correction of $^{129}Xe^+$ and $^{127}I^{1}H_2{}^+$. The availability of tandem quadrupole ICP-MS (ICP-QMS/QMS) with a reaction cell permitted the measurement of ^{129}I at so-called mass-shift mode,[25] i.e., $^{129}I^+$ passed through the first quadrupole (mass to charge ratio (m/z) set to 129) and reacted with the cell gas to form $^{129}I^{16}O^+$, which passed through the second quadrupole (m/z set to 145). This mass-shift mode measurement can be more effective for separating spectral interferences in ^{129}I measurement by ICP-MS. However, the yield of $^{129}I^{16}O^+$ from oxygen reaction with $^{129}I^+$ was relatively low (under 20%) given that the reaction is endothermic ($\Delta H = 2.8$ eV, approximately 270 kJ/mol).[44] Efforts to improve the yield of $^{129}I^{16}O^+$ were attempted by the introduction of more reactive gases, such as CO_2 and N_2O, but neither showed positive effect.[25]

Recently, one of the present authors (Y.Z.) reported a concise yet comprehensive study on using ozone as a cell gas for ICP-QMS/QMS, examining its effects on most chemical elements with stable isotopes in the periodic table.[45] The findings showed that ozone significantly enhances the yield of $^{127}I^{16}O^+$ from $^{127}I^+$ when compared to oxygen. In the current study, the authors focus on a detailed investigation of the measurement of ^{129}I using ICP-QMS/QMS with ozone as the cell gas, aiming to improve the separation of related spectral interferences

[1]National Metrology Institute of Japan, National Institute of Advanced Industrial Sciences and Technology, 1-1-1 Umezono, Tsukuba, Ibaraki 305-8563, Japan
[2]Lead contact
*Correspondence: yb-zhu@aist.go.jp (Y.Z.), d.asakawa@aist.go.jp (D.A.)
https://doi.org/10.1016/j.isci.2024.111138

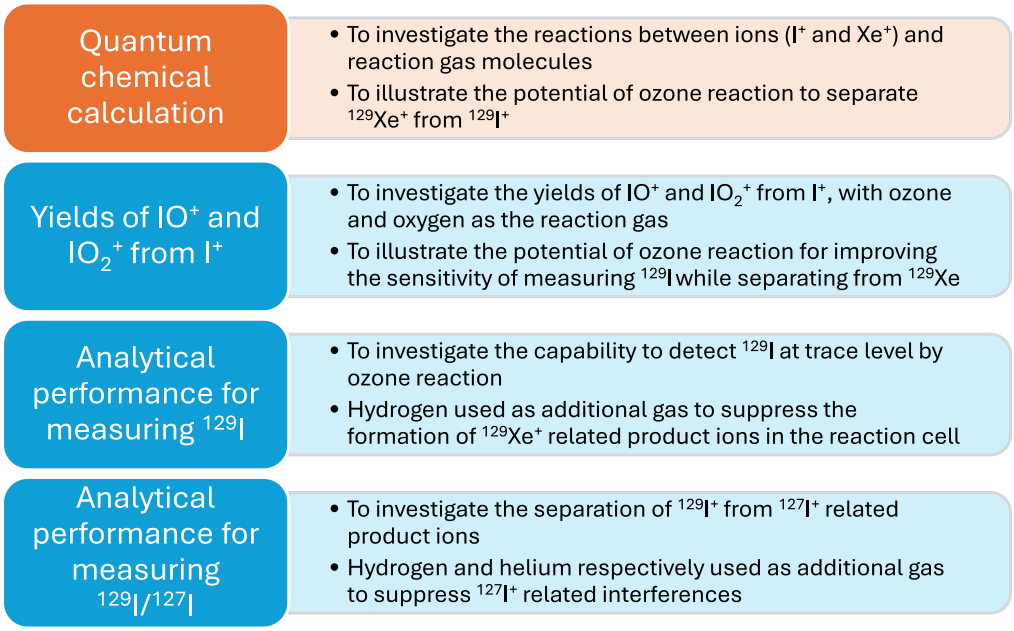

Figure 1. Major studies and objectives of the present work

and enhance isotopic analysis capabilities. Additionally, quantum chemical calculations were performed to elucidate the mechanisms of reactions between iodine ions and cell gas molecules. The major studies and objectives of this study are illustrated in Figure 1.

RESULTS AND DISCUSSION

Quantum chemical calculations of the reactions of I^+ with oxygen and ozone

To investigate the differences in reactions of I^+ with oxygen and ozone, quantum chemical calculations were performed based on density functional theory.

First, the reaction of I^+ and oxygen was investigated (Figure 2A, blue plots). Herein, I^+ and oxygen were calculated as a triplet, which is the most stable quantum. Furthermore, I^+ and oxygen provided a complex, $I^+(O_2)$, and the corresponding relative energy was −0.27 eV.

Subsequently, IO^+ produced by the cleavage of O–O bond in $I^+(O_2)$ through transition state, TS(I^+-O_2), provided either IO^+ or IO_2^+. The transition state for the corresponding dissociation was calculated and its relative energy was 2.26 eV, indicating a less stable state than the reactants. These results indicate that the low production efficiency of $^{127}I^{16}O^+$ and $^{127}I^{16}O_2^+$ using oxygen as cell gas can be attributed to the high transition state barrier.

Next, the reaction of I^+ and ozone was investigated (Figure 2A and 2B, red plots). Regarding the reaction of I^+ and ozone, IO_2^+ was generated by sequential reactions through IO^+. Similar to the reaction with oxygen, I^+ also provided a complex with ozone. However, the corresponding complex, $I^+(O_3)$ with relative energy of −0.86 eV, was more stable than the reactants. Then, $I^+(O_3)$ produced IO^+ and O_2 via transition state and TS(I^+-O_3) with relative energy of −0.02 eV. This was more stable than the reactants. Given that IO^+ and O_2 were more stable than I^+ and O_3 by relative energy of 2.88 eV, the reaction between I^+ and O_3 proceeded as a barrierless process. Subsequently, resultant IO^+ provided a complex with ozone, $IO^+(O_3)$, which undergoes O–O bond cleavage to produce IO_2^+ and O_2 through transition state, TS(IO^+-O_3). Furthermore, $IO^+(O_3)$, TS(IO^+-O_3), and products (IO_2^+ and O_2) were more stable than reactants (IO^+ and O_3) by relative energy of 0.47, 0.24, and 0.62 eV, respectively.

The results of quantum chemical calculations indicate that the use of ozone as reaction gas can efficiently produce IO^+ and IO_2^+ because the reaction of I^+ and IO^+ with ozone proceeded as barrierless processes.

Quantum chemical calculations of the reactions of Xe^+ with ozone

One of the major spectral interferences with the measurement of $^{129}I^+$ is $^{129}Xe^+$. Therefore, density functional theory-based quantum chemical calculation was also performed about the reactions of Xe^+ and ozone to investigate the differences in comparison to I^+.

The Xe^+ and ozone provided a complex, $Xe^+(O_3)$, and the corresponding relative energy was −1.23 eV. Subsequently, XeO^+ and O_2 were produced by the degradation of $Xe^+(O_3)$. The relative energy of the corresponding transition state was −0.25 eV. Additionally, XeO^+ and O_2 were more stable than Xe^+ and O_3 by relative energy of 1.03 eV, indicating that the reaction between Xe^+ and O_3 proceeded as a barrierless process (Figure 3A), similar to the reaction of I^+ and ozone. Therefore, XeO^+ will be obtained as the product ion of the spontaneous and barrierless reaction between Xe^+ and ozone, indicating a spectral interference of $^{129}Xe^{16}O^+$ with the measurement of $^{129}I^{16}O^+$.

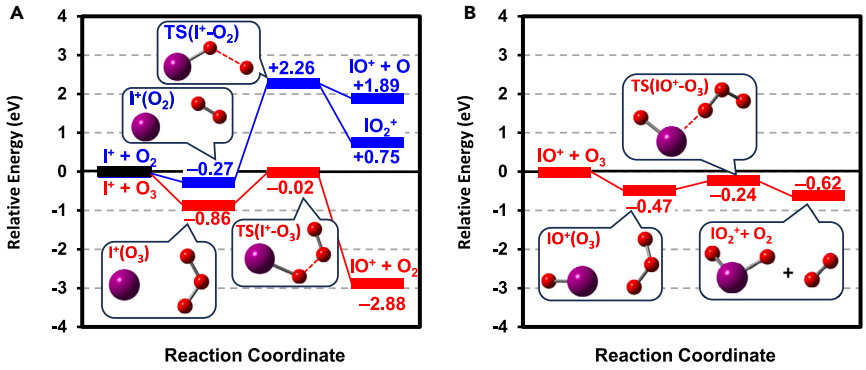

Figure 2. Energy diagrams of the reaction of I^+ with O_2 and O_3, and those of the reaction of IO^+ with O_3

(A) The reaction of I^+ with O_2 (blue plots) and O_3 (red plots).

(B) The reaction of IO^+ with O_3.

Furthermore, XeO_2 might be generated by the reaction between XeO^+ and ozone. The detail of the corresponding reaction pathway is shown in Figure 3B. The ozone interacts with Xe and O atoms in XeO^+ to produce $OXe^+(O_3)$ and $XeO^+(O_3)$, respectively. The relative energy of $OXe^+(O_3)$ and $XeO^+(O_3)$ were −0.65 and −0.44 eV, respectively. The $OXe^+(O_3)$ was produced from XeO_2^+ and O_2 through transition state, $TS(OXe^+\text{-}O_3)$. Notably, the products (XeO_2^+ and O_2) were less stable than the reactants (XeO^+ and O_3) by relative energy of 0.13 eV. Therefore, the formation of XeO_2^+ from XeO^+ and ozone proceeded as endothermic reaction (Figure 3B). The resultant XeO_2^+ can react with oxygen to provide XeO^+ and O_3 because the corresponding reaction occurs as barrierless process. Conversely, the degradation of $Xe^+O(O_3)$ occurred through transition state, $TS(XeO^+\text{-}O_3)$, which was more stable than the reactants by relative energy of 0.35 eV. Therefore, the reaction of XeO^+ and ozone through $Xe^+O(O_3)$ proceeded as exothermic reaction, whereas the product is Xe^+ due to low stability of the complex comprising Xe^+ and O_2. The quantum chemistry calculation strongly suggests that XeO_2^+ is barely produced by the reaction of Xe^+ and ozone. Therefore, the measurement of $^{129}I^{16}O_2^+$ will be significantly less interfered by $^{129}Xe^+$ related ions.

Improved yields of IO^+ and IO_2^+ ions by using ozone as opposed to oxygen as the cell gas for ICP-QMS/QMS

In the present study, online generated ozone was used as cell gas for ICP-QMS/QMS to investigate the product ions from I^+. Ozone was generated by passing dry oxygen gas through the space between a pair of concentric cylindrical quartz electrodes, which were water-cooled to maintain the temperature at 20°C. At the optimized flow rate of oxygen (200 mL/min), stable and high concentration of ozone (approximately 450 g/m^3, gauge pressure 0.1 MPa) can be realized. A 250-min stability test demonstrated a relative standard deviation of less than 1.0%, which is sufficiently low for use as a cell gas in ICP-QMS/QMS, considering that typical measurements often have a relative standard deviation of approximately 1% or higher. The online-generated ozone was split into two branches using a T-connector: one branch directed ozone to the reaction cell of the ICP-QMS/QMS, while the other was connected to a catalytic ozone decomposition device. The ozone flow rate to the reaction cell was controlled by the instrument's built-in mass flow controller, while the flow rate to the decomposition device was regulated by an additional mass flow controller at the under stream. In the present study, the concentration of ozone was approximately 10.5% (v/v) in oxygen matrix. This gas is simply referred as "ozone" in the following text. A comparison of ozone and oxygen as the cell gas for an ICP-QMS/QMS was performed to investigate product ions from $^{127}I^+$. When oxygen was used

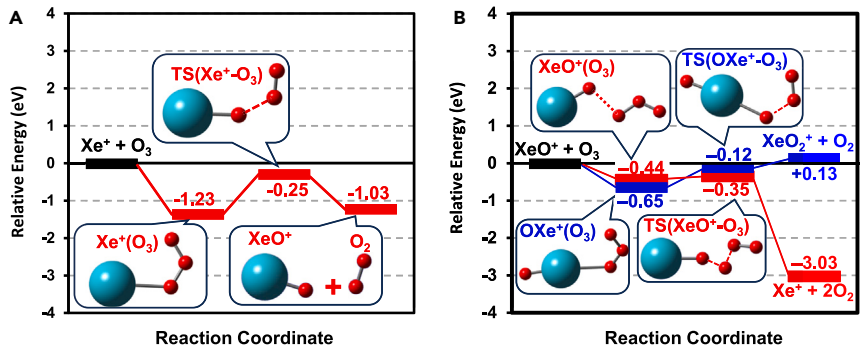

Figure 3. Energy diagrams of the reaction of Xe^+ with O_3 and those of the reaction of XeO^+ with O_3

(A) The reaction of Xe^+ with O_3.

(B) The reaction of XeO^+ with O_3.

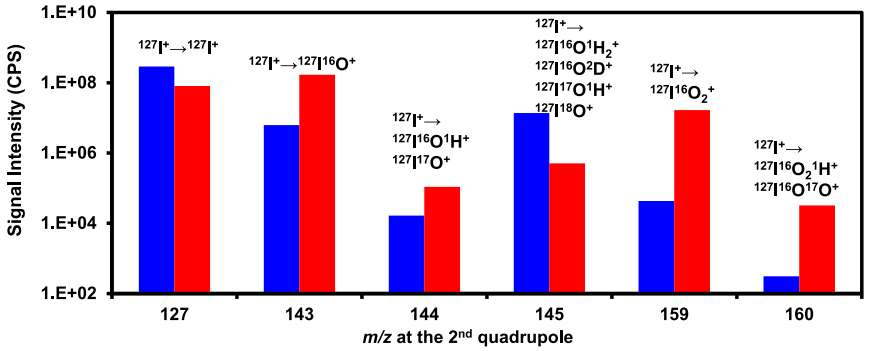

Figure 4. Product ions of $^{127}I^+$ in the reaction cell of ICP-QMS/QMS by reaction with oxygen and ozone, respectively

Cell gas flow rate, 0.2 mL/min; test sample, 10 mg/L of iodine in 2% tetramethyl ammonium hydroxide (TMAH). Blue bar, oxygen as cell gas; red bar, ozone as cell gas.

as the cell gas (Figure 4, blue bar), the dominating product ion was I^+. Furthermore, product ion IO^+ (m/z = 143) was observed but accompanied by $I^{16}OH_2^+$ or $I^{17}OH^+$ or $I^{18}O^+$ (m/z = 145) with a higher signal intensity. It is not surprising that ^{129}I was not measured as $^{129}I^{16}O^+$ in single quadrupole ICP-MS with oxygen as the cell gas,[20,21,23,28–30,32–34,37,39,40,42] majorly due to the interference of $^{127}I^{16}O^1H_2^+$ or $I^{17}OH^+$ or $^{127}I^{18}O^+$ with the measurement of $^{129}I^{16}O^+$. Even by using an ICP-QMS/QMS, ^{129}I was more often measured as $^{129}I^+ \rightarrow {}^{129}I^+$ (both 1st quadrupole and 2nd quadrupole set to permit the passage of an ion with an m/z of 129) but not $^{129}I^+ \rightarrow {}^{129}I^{16}O^+$ (the 1st quadrupole and the 2nd quadrupole set to permit the passage of an ion with an m/z of 129 and 145, respectively).[26,35,38] This occurred despite the exclusion of $^{127}I^+$ from entering the reaction cell. This can be partly attributed to the low yield of IO^+ (approximately 10%) when oxygen was used the cell gas. When ozone was used as the cell gas (Figure 4, red bar), IO^+ (m/z = 143) became the dominating product ion and could be considered as a candidate for measuring iodine at higher sensitivity. Additionally, the apparently high yield of IO_2^+ (m/z = 159) indicates that it can also be another candidate for measuring iodine. These results are in coincidence with the results of quantum chemical calculations provided in Figure 2. Notably, when the ICP-QMS/QMS was operated without introducing any cell gas, only $^{127}I^+$ was observed at the second quadrupole. When oxygen or ozone was introduced as the reaction gas, the sum of the signal intensities for ions observed at the second quadrupole, with m/z of 127, 143, 144, 159, and 160, was approximately equal to that of $^{127}I^+$ observed without any cell gas. This is because the operating conditions for the oxygen or ozone reactions were optimized to maximize the extraction of product ions from the reaction cell, resulting in ion transmission rates similar to those achieved without any cell gas.

Analytical performance of ozone reaction for measurement of ^{129}I

Dependence of signal intensities of I^+, IO^+, and IO_2^+ on ozone flow rate (as reaction cell gas) was investigated in the range from 0.1 to 1.0 mL/min (Figure 5A). With the increase in ozone flow rate, the signal intensity of I^+ decreased gradually to zero at ozone flow rate of approximately 0.5 mL/min. Meanwhile, the signal intensities of IO^+ and IO_2^+ increased gradually to the highest values at ozone flow rates of approximately 0.25 mL/min and 0.35 mL/min, respectively. After reaching the highest values, both signal intensities decreased with the increase in ozone flow rate. The increase in IO^+ and IO_2^+ intensities can be attributed to the increased yield due to increased reactant supply, while the decrease in the intensities can be partly attributed to the deterioration of transmittance due to the increased collisions with cell gas. Ozone flow rate at 0.3 mL/min (dashed line, Figure 5A) was selected as a compromised optimum condition to obtain relatively higher signal intensities for IO^+ and IO_2^+.

The improvement in yields of IO^+ and IO_2^+ by using ozone as the cell gas indicates that highly sensitive measurement of $^{129}I^+$ can be performed in mass-shift mode. Further studies on the reagent blank values (2% TMAH, Figure 5B, sample no. 1) showed that apparent signals were observed at m/z for both types of ions ($^{129}I^{16}O^+$ and $^{129}I^{16}O_2^+$) measured for $^{129}I^+$. Addition of 10 μg/mL ^{127}I in the reagent blank did not result in higher blank signals (2% TMAH, Figure 5B, sample no. 2), indicating their major source was not $^{127}I^1H_2^+$. The blank equivalent concentrations (BECs) observed at $^{129}I^{16}O^+$ and $^{129}I^{16}O_2^+$ were 3.8 and 0.4 pg/mL, respectively, approximately 2 and 3 orders of magnitude lower than the sample with 1.0 ng/mL ^{129}I (Figure 5B, sample no. 3), respectively.

A study on the product ions of Xe isotopes showed that XeO^+ and XeO_2^+ were both observed. Signal intensities for Xe^+, XeO^+, and XeO_2^+ (Figure 5C and 5D) observed at different mass numbers (129, 130–132, 134, and 136) of Xe isotopes agreed with the natural isotope abundances of Xe.[46] It should be noted that the signal intensities of XeO_2^+ (Figure 5D) were over one order of magnitude lower than those of XeO^+ (Figure 5C, green plots), approximately in proportion to the blank signals observed in Figure 5B. Therefore, the blank signals observed for measuring $^{129}I^{16}O^+$ and $^{129}I^{16}O_2^+$ can be attributed to the contribution of $^{129}Xe^{16}O^+$ and $^{129}Xe^{16}O_2^+$, respectively. The much lower signal intensities of XeO_2^+ than those of Xe^+ and XeO^+ are in coincidence with the results of quantum chemical calculations given in Figure 3.

To achieve free-of-spectral-interference measurements of ^{129}I, hydrogen was additionally introduced as the cell gas along with 0.3 mL/min ozone. The results showed that the signal intensities of $^{129}Xe^{16}O^+$ observed for blank samples significantly decreased with the increase in hydrogen flow rate (Figure 6A). Meanwhile, the signal intensities of $^{129}Xe^{16}O_2^+$ also slightly decreased with the increase in hydrogen flow rate.

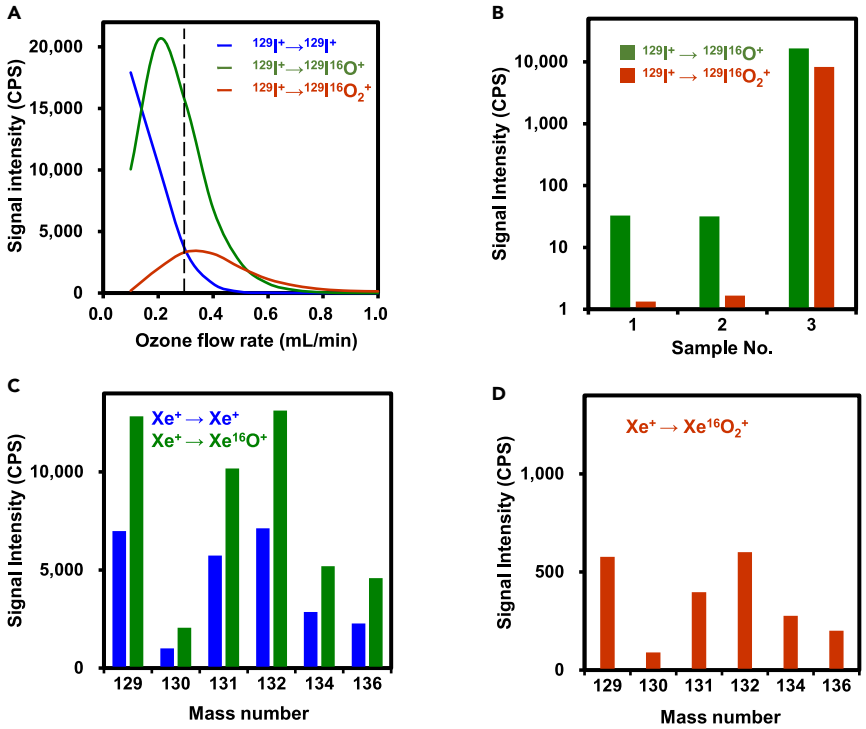

Figure 5. Product ions of I^+ and Xe^+ from the reactions with ozone

(A) Dependence of signal intensities of I^+, IO^+, and IO_2^+ on ozone flow rate. Test sample, 1.0 ng/mL ^{129}I in 2% TMAH.

(B) Signal intensities of IO^+ and IO_2^+ observed for measuring $^{129}I^+$. Sample 1, 2% TMAH; sample 2, 2% TMAH with 10 μg/mL ^{127}I; sample 3, 2% TMAH with 10 μg/mL ^{127}I and 1.0 ng/mL ^{129}I. Cell gas, ozone 0.3 mL/min, same below.

(C) Product ions of Xe isotopes, $Xe^+ \rightarrow Xe^+$(blue plots) and $Xe^+ \rightarrow Xe^{16}O^+$ (green plots).

(D) Product ions of Xe isotopes, $Xe^+ \rightarrow Xe^{16}O_2^+$.

The signal intensity of $^{129}I^{16}O^+$ (Figure 6B, achieved with 1.0 ng/mL ^{129}I) also decreased gradually with the increase in hydrogen flow rate, from approximately 16,000 counts per second (CPS) at 0 mL/min of hydrogen to approximately 5,000 CPS at 10 mL/min of hydrogen. Conversely, the change in signal intensity of $^{129}I^{16}O_2^+$ due to increased hydrogen flow rate was much less significant than that of $^{129}I^{16}O^+$. These results may be attributed to this fact: reaction of ($^{129}I^{16}O^+ + H_2 \rightarrow {}^{129}I^+ + H_2{}^{16}O$) is more likely to occur than ($^{129}I^{16}O_2^+ + 2H_2 \rightarrow {}^{129}I^+ + 2H_2{}^{16}O$). It should be noted that the BEC values observed for $^{129}I^{16}O^+$ and $^{129}I^{16}O_2^+$ at 10 mL/min of hydrogen were 0.016 pg/mL and 0.019 pg/mL, respectively.

The concentrations of ^{129}I in multiple water samples were determined with the method (Figure 6C) proposed in this study. The concentration in each original sample was under the detection limit, while the observed values (both measured by $^{129}I^{16}O^+$ and $^{129}I^{16}O_2^+$) of ^{129}I spiked samples were in good agreement with the concentrations spiked (level one of 70 pg/mL, and level two of 134 pg/mL). These results were obtained with a relative standard deviation of approximately 2%–7%. The guidance level for ^{129}I in drinking water established by the World Health Organization (WHO) is 1 Bq/L,[47] equivalent to a concentration of 152.9 pg/mL. Detection limit (to be discussed in the following text), BEC, and reproducibility achieved in the present study are sufficiently good for fulfilling the WHO guidance for ^{129}I. It should be noted that the detection limit and BEC were four orders of magnitude under the guidance level, permitting precise measurement of 100-times diluted seawater for monitoring ^{129}I at the WHO guidance level. Polyatomic ions, such as $^{89}Y^{40}Ar^+$, $^{97}Mo^{16}O_2^+$, and $^{113}Cd^{16}O^+$, can be potential spectral interferences for the measurement of $^{129}I^+$ by ICP-MS.[25,26,37,38] A test with single-element standard solutions Y, Mo, and Cd (10 μg/mL each) showed that spectral interferences from these elements were negligible in the current study.

To date, over 20 studies reported quantitative analysis of ^{129}I by ICP-MS.[20–43] Detection limits (concentration equivalent to 3-fold standard deviation of the blank) reported before the application of reaction/collision cell exceeded 30 pg/mL (Table 1).[24,27,36] This is primarily attributable to the interference from ^{129}Xe as impurities in argon gas. The introduction of reaction/collision cell technique improved the detection limit to sub pg/mL level.[23,25,29,30,35] However, typical BECs still exceeded 2 pg/mL.[19,25,37,38,40] This can potentially be explained by the insufficient reaction of $^{129}Xe^+$ with cell gas (O_2). It should be noted that mass-shift measurement ($^{129}I^+ \rightarrow {}^{129}I^{16}O^+$) was also reported with a BEC of 2.9 pg/mL, which potentially indicates the formation of $^{129}Xe^{16}O^+$. Another drawback of using O_2 as the cell gas for mass-shift measurement of $^{129}I^+$ is that the yield of $^{129}I^{16}O^+$ is approximately 10%, resulting in a lower sensitivity when compared to the measurement by $^{129}I^+$. The introduction of more-reactive gases, such as N_2O and CO_2, failed to improve the yield of $^{129}I^{16}O^+$. In the current study, the introduction of ozone as

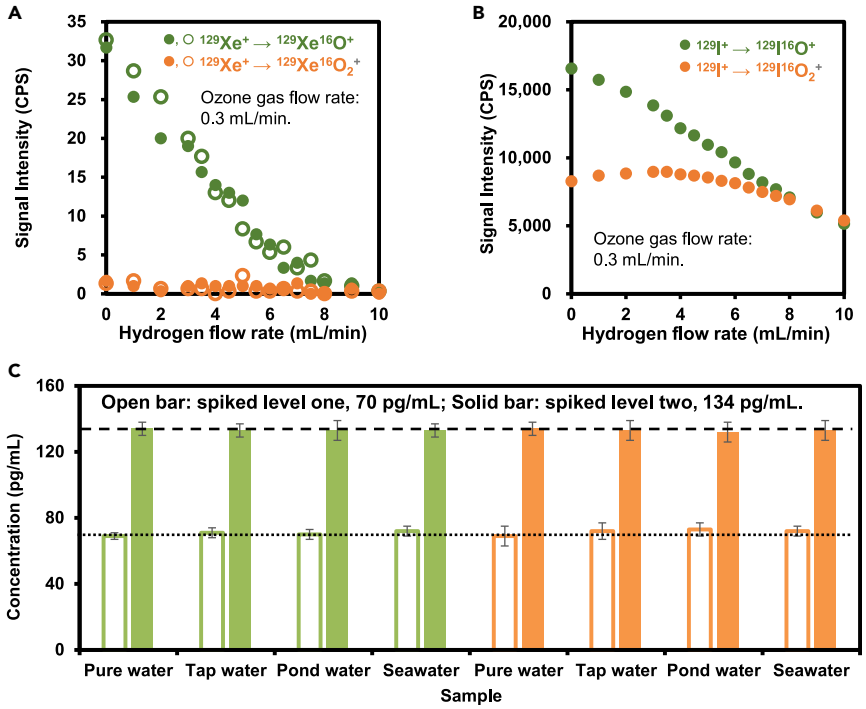

Figure 6. Results for hydrogen flow rate optimization and those for the determination of ^{129}I in natural water samples

(A) Dependence of signal intensities observed for $^{129}Xe^+ \rightarrow {}^{129}Xe^{16}O^+$ and $^{129}Xe^+ \rightarrow {}^{129}Xe^{16}O_2{}^+$ on flow rate of hydrogen as additional cell gas. Samples: open plots, 2% TMAH; solid plots, 2% TMAH with 10 μg/mL ^{127}I.

(B) Dependence of signal intensities observed for $^{129}I^+ \rightarrow {}^{129}I^{16}O^+$ and $^{129}I^+ \rightarrow {}^{129}I^{16}O_2{}^+$ on flow rate of hydrogen as additional cell gas. Sample, 2% TMAH with 10 μg/mL ^{127}I and 1.0 ng/mL ^{129}I.

(C) Observed values of ^{129}I in spiked natural water samples. Green plots, measured with $^{129}I^+ \rightarrow {}^{129}I^{16}O^+$; orange plots, measured with $^{129}I^+ \rightarrow {}^{129}I^{16}O_2{}^+$, plots show (mean ± standard deviation, n = 10). Dotted line, spiked level one; dashed line, spiked level two. Cell gas, ozone 0.3 mL/min, hydrogen 10 mL/min.

cell gas improved the yields of $^{129}I^{16}O^+$ and $^{129}I^{16}O_2{}^+$, both of which can be used for the measurement of ^{129}I. The signals of $^{129}Xe^{16}O^+$ and $^{129}Xe^{16}O_2{}^+$ were effectively suppressed by introducing hydrogen as an additional cell gas. The detection limits by measuring $^{129}I^{16}O^+$ and $^{129}I^{16}O_2{}^+$ were 0.062 and 0.057 pg/mL with BECs of 0.016 and 0.019 pg/mL (H_2 flow rate, 10 mL/min), respectively. The detection limits and BECs obtained in the current study, with O_2 (or O_2 and H_2) as the cell gas, are also listed in Table 1 for comparison. The measurement of $^{129}I^+ \rightarrow {}^{129}I^+$ with O_2 and H_2 as the cell gas resulted in much lower detection limit and BEC than those obtained solely with O_2. However, the detection limits and BECs obtained by measuring $^{129}I^{16}O^+$ and $^{129}I^{16}O_2{}^+$ with O_3 as the reaction gas showed the best performance. Notably, in case of samples with high concentration of ^{127}I (e.g., over 50 mg/L for isotopic ratio analysis of $^{129}I/^{127}I$), the introduction of H_2 along with O_2 can result in a higher blank for $^{129}I^+$ due to the interference by $^{127}I^1H_2{}^+$(e.g., Table 2, 1.5×10^{-8} increased to 4.6×10^{-7} for the measurement of $(^{129}I^+ \rightarrow {}^{129}I^+)/(^{127}I^+ \rightarrow {}^{127}I^+)$. Therefore, it is not surprising that H_2 was not used with O_2 in the studies reported to date.

Analytical performance of ozone reaction for measurement of $^{129}I/^{127}I$ isotopic ratio

In addition to the quantitative analysis of ^{129}I in samples, the isotopic ratio of $^{129}I/^{127}I$ is frequently measured to evaluate the contribution of anthropogenic ^{129}I to the environment. However, the extraction of ^{129}I in natural samples is always accompanied by relatively high concentration of ^{127}I due to the similarity in chemical properties.

High concentration of iodine solutions are usually used to check the capability for analyzing isotopic ratio at extremely low $^{129}I/^{127}I$ values, e.g., from 63.5 to 5,000 μg/mL of natural iodine (Table 2). A preliminary test in the current study showed that when the concentration of iodine (^{127}I) exceeds 1,000 μg/mL, the slope of the calibration curve decreases for each ^{127}I related ion such as $^{127}I^+ \rightarrow {}^{127}I^{16}O^+$, $^{127}I^+ \rightarrow {}^{127}I^{18}O^+$(or $^{127}I^{17}O^1H^+$, $^{127}I^{16}O^1H_2{}^+$), and $^{127}I^+ \rightarrow {}^{127}I^{16}O_2{}^+$. This potentially indicates that the ionization rate of iodine decreases at high concentrations. Therefore, the concentration of natural iodine was set to 500 μg/mL for measuring $^{129}I/^{127}I$ ratio.

The isotopic ratios of $^{129}I/^{127}I$ observed for 500 μg/mL of natural iodine were 4.4×10^{-8} (Table 2) when the measured ions were $(^{129}I^+ \rightarrow {}^{129}I^{16}O^+)$ and $(^{127}I^+ \rightarrow {}^{127}I^{16}O^+)$, respectively, independent to the use of H_2 or He as the additional cell gas to O_3. It should be noted that when the 1st quadrupole was set to permit the passage of ions with m/z of 129, $^{127}I^1H_2{}^+$ also can pass and enter the reaction cell along with $^{129}I^+$. The reaction of $^{127}I^1H_2{}^+$ with O_3 results in the formation of $^{127}I^{18}O^+$, which can pass the 2nd quadrupole set to permit the passage ions with m/z of 145 and arrive at the detector, overlapping with the spectrum of $^{129}I^{16}O^+$. Furthermore, the ratio of signal intensity observed at $(^{129}I^+$(or $^{127}I^1H_2{}^+) \rightarrow {}^{129}I^{16}O^+$(or $^{127}I^{18}O^+$)) to that observed at $(^{129}I^+$(or $^{127}I^1H_2{}^+) \rightarrow {}^{127}I^{16}O^+$) was approximately 0.21% and close to the isotopic

Table 1. Typically reported detection limits for ^{129}I achieved with ICP-MS

Year	ICP-MS model	Cell gas	Measured ion	Detection limit (pg/mL)	Reference
1992	PlasmaQuad PQ2	NA[a]	$^{129}I^+$	30	Cox et al.[36]
1995	Yokokawa PMS-2000.	NA[a]	$^{129}I^+$	76	Marumatsu and Yoshida[24]
1996	ELEMENT	NA[a]	$^{129}I^+$	50	Kerl et al.[27]
2003	Platform ICP	O_2, He	$^{129}I^+$	0.8	Izmer et al.[30]
2004	Platform ICP	O_2, He	$^{129}I^+$	0.4	Izmer et al.[29]
2005	ELAN DRC II	O_2	$^{129}I^+$	10	Brown et al.[39]
2007	ELAN DRC II	O_2	$^{129}I^+$	5.7[3.2][b]	Brown et al.[40]
2011	ELAN DRCe	O_2	$^{129}I^+$	15.2	Fujiwara et al.[33]
2013	Agilent 8800	O_2	$^{129}I^+$	0.3[c]	Ohno et al.[23]
2013	Agilent 7700x	O_2	$^{129}I^+$	1.5	Ohno et al.[22]
2014	Agilent 7500a	NA[a]	$^{129}I^+$	14.73	Hsieh et al.[31]
2014	ELEMENT 2	NA[a]	$^{129}I^+$	0.7	Ezerinskis et al.[35]
2018	Agilent 8800	O_2	$^{129}I^+$	1.5	Yang et al.[20]
2021	iCAP RQ	O_2	$^{129}I^+$	1.81	Kimmig et al.[26]
2022	NexION 5000	O_2, CO_2	$^{129}I^+$	0.11[14][b]	Matsueda et al.[25]
2022	Agilent 8900	O_2	$^{129}I^+ \rightarrow {}^{129}I^{16}O^+$	1.7[2.9][b]	Clralie et al.[37]
2022	iCAP RQ	O_2	$^{129}I^+$	1.11[8][b]	Chang et al.[38]
2023	Agilent 8800	O_2	$^{129}I^+$	17[4][b]	Zacharauskas et al.[19]
Present	Agilent 8800	O_2	$^{129}I^+$	0.7[2.4][b]	Present work
		O_2	$^{129}I^+ \rightarrow {}^{129}I^{16}O^+$	5[10][b]	
		O_2, H_2	$^{129}I^+$	0.12[0.13][b]	
		O_2, H_2	$^{129}I^+ \rightarrow {}^{129}I^{16}O^+$	4[0.8][b]	
		O_3, H_2	$^{129}I^+ \rightarrow {}^{129}I^{16}O^+$	0.062[0.016][b]	
			$^{129}I^+ \rightarrow {}^{129}I^{16}O_2^+$	0.057[0.019][c]	

[a]Not available.
[b]BEC given in square brackets.
[c]Estimated as 0.3-fold of quantitation limit.

ratio of $^{18}O/^{16}O$ in natural oxygen gas. Therefore, the relatively high isotopic ratio of $^{129}I/^{127}I$ observed by measuring ($^{129}I^+ \rightarrow {}^{129}I^{16}O^+$) and ($^{127}I^+ \rightarrow {}^{127}I^{16}O^+$) can be primarily attributed to the spectral interferences from ($^{127}I^1H_2^+ \rightarrow {}^{127}I^{18}O^+$) to ($^{129}I^+ \rightarrow {}^{129}I^{16}O^+$).

Conversely, when the measured ions were ($^{129}I^+ \rightarrow {}^{129}I^{16}O_2^+$) and ($^{127}I^+ \rightarrow {}^{127}I^{16}O_2^+$), the isotopic ratios of $^{129}I/^{127}I$ observed for 500 μg/mL of natural iodine were 4.9×10^{-9} and 6.7×10^{-10} (Table 2) by using H_2 and He as the additional cell gas to O_3, respectively. These lower isotopic ratios can be attributed to the exclusion of ^{18}O related spectral interferences. Besides, the relatively higher isotopic ratio obtained with H_2 than that obtained with He probably can be attributed to the formation of $^{127}I(^{16}O^1H_2)^+$ through the reaction of $^{127}I^1H_2^+$ with O_3. The results for isotopic ratio of $^{129}I/^{127}I$ in natural iodine solutions spiked with varying levels of ^{129}I (Figure 7) were in good agreement with the estimated values. Notably, the results obtained by measuring ($^{127}I^+ \rightarrow {}^{127}I^{16}O^+$) were corrected with reagent blank values provided in Table 2.

Multiple studies based on ICP-QMS/QMS reported the performance for measuring isotopic ratio of $^{129}I/^{127}I$ (Table 2). The lowest values were realized at approximately 4×10^{-9} to 7×10^{-9}, which can be attributed to $^{127}I^1H_2^+$ (with minor contribution from $^{127}I^2D^+$) related to spectral interferences.[20,25,28]

A report claimed that 4.6×10^{-10} can be realized for isotopic ratio of $^{129}I/^{127}I$ by using 5,000 μg/mL of ^{127}I solution,[25] with approximately 2×10^{-9} in 1,000 μg/mL of ^{127}I solution. The best performance (by measuring $I^+ \rightarrow I^{16}O_2^+$, with O_3 and He as the cell gas) in the current study realized 6.7×10^{-10} for isotopic ratio of $^{129}I/^{127}I$ by using 500 μg/mL of ^{127}I solution. Assuming the signal intensity for ^{127}I in 5,000 μg/mL of ^{127}I with the present methods, the ratio of $^{129}I/^{127}I$ can be realized as low as 6.7×10^{-11}, approximately one order of magnitude lower than that reported.

The results obtained with O_2 as the cell gas are also summarized in Table 2 for comparison. When O_2 was used as the cell gas, the performances by measuring ($I^+ \rightarrow I^{16}O^+$) and ($I^+ \rightarrow I^{16}O_2^+$) were even worse than those obtained by measuring ($I^+ \rightarrow I^+$), attributable to low sensitivities due to the low yields of $I^{16}O^+$ and $I^{16}O_2^+$. The use of additional H_2 or He failed in improving the analytical performance.

The reactions about $^{129}I^+$, $^{127}I^1H_2^+$, and $^{129}Xe^+$ in reported studies and the present study are illustrated in Figures 8A–8D. In reported studies, both the on-mass measurements (Figure 8A) and mass-shift measurements (Figure 8B) failed to completely remove the interference from $^{127}I^1H_2^+$ and $^{129}Xe^+$ to $^{129}I^+$, or $^{127}I^{18}O^+$ and $^{129}Xe^{16}O^+$ to $^{129}I^{16}O^+$. The introduction of O_3 and H_2 as cell gas provided more efficient

Table 2. Performance for measuring $^{129}I/^{127}I$ achieved with ICP-QMS/QMS

Year	ICP-MS model	Cell gas	Measured ion	$^{129}I/^{127}I$	^{127}I (μg/mL)	Reference
2013	Agilent 8800	O_2	$I^+ \rightarrow I^+$	5×10^{-9}	100	Ohno et al.[23]
2018	Agilent 8800	O_2	$I^+ \rightarrow I^+$	6.95×10^{-9}	63.5	Yang et al.[20]
2022	NexION 5000	O_2, CO_2	$I^+ \rightarrow I^+$	4.6×10^{-10}	5000	Matsueda et al.[25]
				$\approx 2 \times 10^{-9}$	1000	
2022	Agilent 8900	O_2	$I^+ \rightarrow I^{16}O^+$	3.8×10^{-9}	NA[a]	Coralie et al.[37]
Present	Agilent 8800	O_2	$I^+ \rightarrow I^+$	1.5×10^{-8}	500	Present work
		O_2	$I^+ \rightarrow I^{16}O^+$	1.6×10^{-7}		
		O_2	$I^+ \rightarrow I^{16}O_2^+$	1.2×10^{-6}		
		O_2, H_2	$I^+ \rightarrow I^+$	4.6×10^{-7}		
		O_2, H_2	$I^+ \rightarrow I^{16}O^+$	6.5×10^{-7}		
		O_2, H_2	$I^+ \rightarrow I^{16}O_2^+$	1.9×10^{-6}		
		O_2, He	$I^+ \rightarrow I^+$	1.9×10^{-8}		
		O_2, He	$I^+ \rightarrow I^{16}O^+$	9.3×10^{-7}		
		O_2, He	$I^+ \rightarrow I^{16}O_2^+$	1.5×10^{-6}		
		O_3, H_2	$I^+ \rightarrow I^{16}O^+$	4.4×10^{-8}		
		O_3, H_2	$I^+ \rightarrow I^{16}O_2^+$	4.9×10^{-9}		
		O_3, He	$I^+ \rightarrow I^{16}O^+$	4.4×10^{-8}		
		O_3, He	$I^+ \rightarrow I^{16}O_2^+$	6.7×10^{-10}		

[a]Not available.

removal of interferences from $^{127}I^1H_2^+$ and $^{129}Xe^+$ to $^{129}I^+$ by the measurement of $^{129}I^+ \rightarrow {}^{129}I^{16}O^+$ (Figure 8C) and $^{129}I^+ \rightarrow {}^{129}I^{16}O_2^+$ (Figure 8D), respectively. Furthermore, the measurement of ($^{129}I^+ \rightarrow {}^{129}I^{16}O_2^+$) avoided the interference from $^{127}I^1H_2^+$ related ions, such as $^{127}I^{16}O_2^+$ and $^{127}I^{16}O^{18}O^+$. In the current study, the typical sensitivity (both $^{129}I^{16}O^+$ and $^{129}I^{16}O_2^+$) for measuring ^{129}I were approximately 6,500 CPS for 1.0 ng/mL solution, apparently higher than those reported by measuring $^{129}I^+$ with O_2 (and CO_2) as the cell gas, approximately 300–600 CPS.[26,39] Improvement of sensitivity for measuring ^{129}I can be achieved by modification of the sample matrix,[25,38] attributable to the improvement in iodine ionization in the plasma.

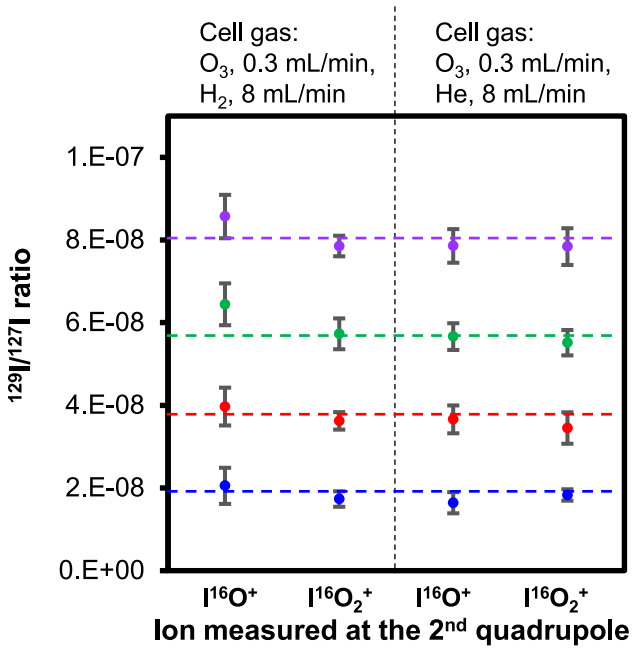

Figure 7. Isotopic ratio of $^{129}I/^{127}I$ in ^{129}I spiked natural iodine sample solution measurement by ICP-QMS/QMS

Test sample, ^{129}I spiked 500 μg/mL iodine (as NH_4I) in 2% TMAH. Plots show (mean ± standard deviation, $n = 10$). Color dashed lines estimated isotopic ratio based on the quantity of ^{129}I and that of natural iodine.

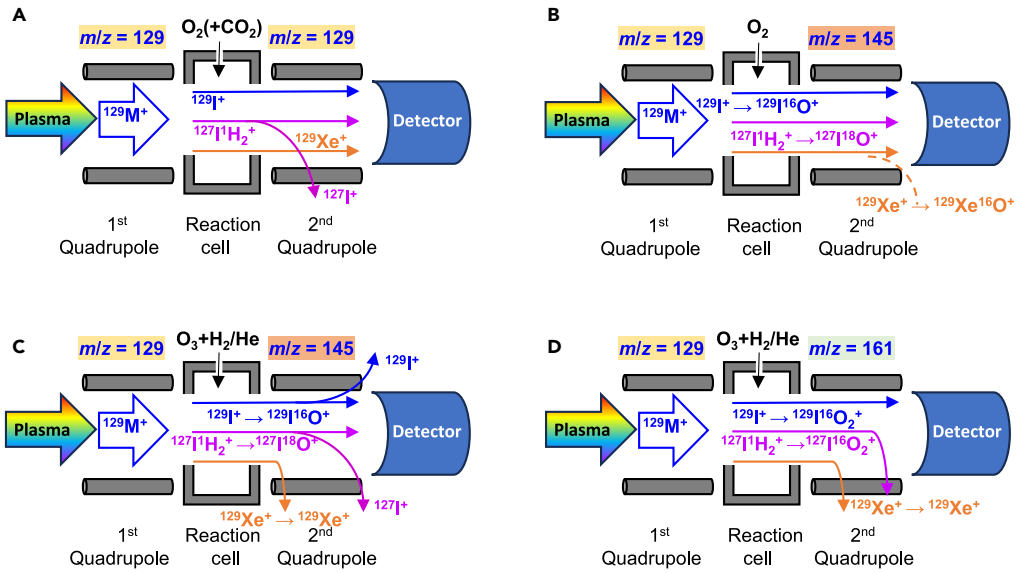

Figure 8. Mechanisms for separating spectral interferences

(A) On-mass measurement of $^{129}I^+$ with O_2(or together with CO_2) as reaction gas.

(B) Mass-shift measurement of $^{129}I^+$(→ $^{129}I^{16}O^+$) with O_2 as reaction gas.

(C) Mass-shift measurement of $^{129}I^+$(→ $^{129}I^{16}O^+$) with O_3 and H_2 (or He) as reaction gases.

(D) Mass-shift measurement of $^{129}I^+$(→ $^{129}I^{16}O_2^+$) with O_3 and H_2 (or He) as reaction gases.

Conclusion

Quantum chemical calculations of reaction enthalpies related to I^+ and Xe^+ indicate that ozone can be used as a cell gas for ICP-QMS/QMS to separate spectral interferences in the measurement of $^{129}I^+$.

Experiments were conducted by using online generated ozone as the reaction gas for ICP-QMS/QMS, where significant improvement of reactions ($^{129}I^+ \rightarrow {}^{129}I^{16}O^+$) and ($^{129}I^+ \rightarrow {}^{129}I^{16}O_2^+$) were observed in comparison to the results with oxygen as the reaction gas. This approach enhances the highly sensitive measurement of $^{129}I^+$ as $^{129}I^{16}O^+$ and $^{129}I^{16}O_2^+$ after ion-molecule reactions. The introduction of hydrogen, as an additional cell gas to ozone, resulted in free-of-spectral-interference measurement of ^{129}I without mathematical correction due to the efficient removal of spectral interferences related to $^{129}Xe^+$.

The measurement of ($^{129}I^+ \rightarrow {}^{129}I^{16}O_2^+$)/($^{127}I^+ \rightarrow {}^{127}I^{16}O_2^+$) resulted in a much lower blank ratio for $^{129}I/^{127}I$ analysis, which can be attributed to the avoidance of $^{127}I^1H_2^+$ related spectral interferences. This occurred in the measurement of ($^{129}I^+ \rightarrow {}^{129}I^{16}O^+$)/($^{127}I^+ \rightarrow {}^{127}I^{16}O^+$). The use of ozone as cell gas for ICP-QMS/QMS provided excellent performance for quantitative analysis of ^{129}I and $^{129}I/^{127}I$ isotopic analysis.

The best performance for quantitative analysis ^{129}I was realized by measuring ($^{129}I^+ \rightarrow {}^{129}I^{16}O^+$) with ozone and additional hydrogen as the reaction gas, obtaining a detection limit of 0.062 pg/mL and a BEC of 0.016 pg/mL, respectively. These results are significantly improved when compared to those reported to date, with the lowest values of 0.11 and 2.9, respectively.

The best performance for analysis of $^{129}I/^{127}I$ ratio was realized by measuring ($^{129}I^+ \rightarrow {}^{129}I^{16}O_2^+$)/($^{127}I^+ \rightarrow {}^{127}I^{16}O_2^+$) with ozone and additional helium as the reaction gas, obtaining a value of 6.7×10^{-10} with 500 μg/mL natural iodine. This can be approximately improved by one order of magnitude when compared to the best results reported to date.

Ozone reaction can improve the formation of MO^+ ion for most elements in the periodic table. It can be expected that there will be more studies on ozone reactions with ions in the following years for separating spectral interferences or other applications.

Limitations of the study

(1) The present study is based on an ICP-QMS/QMS of model Agilent 8800s (compatible with Agilent 8900). Performance for separating spectral interference in measuring ^{129}I can differ slightly when other models of ICP-QMS/QMS are used.

(2) With respect to ICP-QMS/QMS used in the current study, the upper counting limit of the detector and its linearity around this limit are key factors affecting the lower limit achieved for $^{129}I/^{127}I$ ratio.

RESOURCE AVAILABILITY

Lead contact

Further information and requests for resources should be directed to and will be fulfilled by the lead contact, Yanbei Zhu (yb-zhu@aist.go.jp).

Materials availability

This study did not generate new unique reagents.

Data and code availability

- All data generated or analyzed during this study are included in the manuscript and supplementary tables and figures.
- This study does not generate new code.
- Additional information required for reproducing the data reported in this article is available from the lead contact on request.

ACKNOWLEDGMENTS

This study was supported by JSPS KAKENHI (grant number 22K05181, 24K01394). Molecular structure computations were performed at the Research Center for Computational Science in Okazaki, Japan (project no.23-IMS-C066). We would like to thank Editage (www.editage.jp) for English language editing.

AUTHOR CONTRIBUTIONS

The manuscript was collaboratively written by both authors. Quantum chemical calculations were conducted by D.A. Experiments with ICP-QMS/QMS were conducted by Y.Z.

DECLARATION OF INTERESTS

The authors declare no competing interests.

STAR★METHODS

Detailed methods are provided in the online version of this paper and include the following:

- KEY RESOURCES TABLE
- EXPERIMENTAL MODEL AND STUDY PARTICIPANT DETAILS
- METHOD DETAILS
- QUANTIFICATION AND STATISTICAL ANALYSIS
- ADDITIONAL RESOURCES

SUPPLEMENTAL INFORMATION

Supplemental information can be found online at https://doi.org/10.1016/j.isci.2024.111138.

Received: July 30, 2024
Revised: August 28, 2024
Accepted: October 7, 2024
Published: October 21, 2024

REFERENCES

1. Elmore, D., Gove, H.E., Ferraro, R., Kilius, L.R., Lee, H.W., Chang, K.H., Beukens, R.P., Litherland, A.E., Russo, C.J., Purser, K.H., et al. (1980). Determination of I-129 Using Tandem Accelerator Mass-Spectrometry. Nature *286*, 138–140. https://doi.org/10.1038/286138a0.
2. Moran, J.E., Fehn, U., and Teng, R.T. (1998). Variations in 129I/127I ratios in recent marine sediments: evidence for a fossil organic component. Chem. Geol. *152*, 193–203. https://doi.org/10.1016/S0009-2541(98)00106-5.
3. Fan, Y., Zhou, W., and Hou, X. (2018). Pre-nuclear level of 129I in Chinese loess-paleosol sections: A search for the natural 129I level for dating in terrestrial environments. Geochim Cosmochim Ac *231*, 64–72. https://doi.org/10.1016/j.gca.2018.04.014.
4. Fan, Y., Zhang, L., Lan, J., Hou, X., and Zhou, W. (2021). Pre-nuclear values for 129I/127I in Chinese sediments and their geochronological implications. Palaeogeogr Palaeocl *568*, 110312. https://doi.org/10.1016/j.palaeo.2021.110312.
5. Fan, Y., Cheng, P., Negri, A., Lan, J., Liu, X., Zhou, W., Liu, Q., and Hou, X. (2024). Climate Control of Iodine Isotopic Composition Evidenced by Argentine Entisols Records. Geophys. Res. Lett. *51*, e2023GL107811. https://doi.org/10.1029/2023GL107811.
6. Zhang, L., Fang, M., Zhang, T., Jiang, H., Zhang, M., and Hou, X. (2021). Determination of iodine-129 in twenty soil and sediment reference materials. J. Anal. At. Spectrom. *36*, 1544–1553. https://doi.org/10.1039/d1ja00061f.
7. Schnabel, C., Leya, I., Gloris, M., Michel, R., Lopez-Gutiérrez, J.M., Krähenbühl, U., Herpers, U., Kuhnhenn, J., and Synal, H.A. (2004). Production rates and proton-induced production cross sections of 129I from Te and Ba:: An attempt to model the 129I production in stony meteoroids and 129I in a Knyahinya sample. Meteorit. Planet. Sci. *39*, 453–466. https://doi.org/10.1111/j.1945-5100.2004.tb00104.x.
8. Sakaguchi, A., Inaba, R., Sasa, K., Matsunaka, T., Hosoya, S., Takahashi, T., Honda, M., Yamano, H., Sasaki, K., Yamasaki, S., et al. (2018). Reconstruction of anthropogenic 129I temporal variation in the Japan Sea using a coral core sample. Mar. Environ. Res. *142*, 91–99. https://doi.org/10.1016/j.marenvres.2018.09.003.
9. Sahoo, S.K., Muramatsu, Y., Yoshida, S., Matsuzaki, H., and Rühm, W. (2009). Determination of 129I and 127I Concentration in Soil Samples from the Chernobyl 30-km Zone by AMS and ICP-MS. J. Radiat. Res. *50*, 325–332. https://doi.org/10.1269/jrr.08118.
10. Michel, R., Daraoui, A., Gorny, M., Jakob, D., Sachse, R., Tosch, L., Nies, H., Goroncy, I., Herrmann, J., Synal, H.A., et al. (2012). Iodine-129 and iodine-127 in European seawaters and in precipitation from Northern Germany. Sci. Total Environ. *419*, 151–169. https://doi.org/10.1016/j.scitotenv.2012.01.009.
11. Jabbar, T., Steier, P., Wallner, G., Kandler, N., and Katzlberger, C. (2011). AMS analysis of iodine-129 in aerosols from Austria. Nucl Instrum Meth B *269*, 3183–3187. https://doi.org/10.1016/j.nimb.2011.04.023.
12. Hansen, V., Yi, P., Hou, X., Aldahan, A., Roos, P., and Possnert, G. (2011). Iodide and iodate (129I and 127I) in surface water of the Baltic Sea, Kattegat and Skagerrak. Sci. Total Environ. *412–413*, 296–303. https://doi.org/10.1016/j.scitotenv.2011.10.001.
13. Gómez-Guzmán, J.M., Enamorado-Báez, S.M., Pinto-Gómez, A.R., and Abril-Hernández, J.M. (2011). Microwave-based

digestion method for extraction of 129I and 127I from solid material for measurements by AMS and ICP-MS. Int. J. Mass Spectrom. *303*, 103–108. https://doi.org/10.1016/j.ijms.2011.01.006.

14. Fujiwara, H. (2016). Observation of radioactive iodine (131I, 129I) in cropland soil after the Fukushima nuclear accident. Sci. Total Environ. *566–567*, 1432–1439. https://doi.org/10.1016/j.scitotenv.2016.06.004.
15. Daraoui, A., Tosch, L., Gorny, M., Michel, R., Goroncy, I., Herrmann, J., Nies, H., Synal, H.A., Alfimov, V., and Walther, C. (2016). Iodine-129, Iodine-127 and Cesium-137 in seawater from the North Sea and the Baltic Sea. J. Environ. Radioact. *162–163*, 289–299. https://doi.org/10.1016/j.jenvrad.2016.06.006.
16. Bautista, A.T., Miyake, Y., Matsuzaki, H., and Siringan, F.P. (2017). A coral 129I/127I measurement method using ICP-MS and AMS with carrier addition. Anal Methods-Uk *9*, 5181–5188. https://doi.org/10.1039/c7ay01458a.
17. Aldahan, A., Alfimov, V., and Possnert, G. (2007). 129I anthropogenic budget: Major sources and sinks. Appl. Geochem. *22*, 606–618. https://doi.org/10.1016/j.apgeochem.2006.12.006.
18. Hou, X., Hansen, V., Aldahan, A., Possnert, G., Lind, O.C., and Lujaniene, G. (2009). A review on speciation of iodine-129 in the environmental and biological samples. Anal. Chim. Acta *632*, 181–196. https://doi.org/10.1016/j.aca.2008.11.013.
19. Zacharauskas, Ž., Warwick, P., Russell, B., Reading, D., and Croudace, I. (2023). Development of an optimised method for measurement of iodine-129 in decommissioning wastes using ICP-MS/MS. J. Anal. At. Spectrom. *38*, 1431–1441. https://doi.org/10.1039/d3ja00045a.
20. Yang, G., Tazoe, H., and Yamada, M. (2018). Improved approach for routine monitoring of 129I activity and 129I/127I atom ratio in environmental samples using TMAH extraction and ICP-MS/MS. Anal. Chim. Acta *1008*, 66–73. https://doi.org/10.1016/j.aca.2017.12.049.
21. Reid, H.J., Bashammakh, A.A., Goodall, P.S., Landon, M.R., O'Connor, C., and Sharp, B.L. (2008). Determination of iodine and molybdenum in milk by quadrupole ICP-MS. Talanta *75*, 189–197. https://doi.org/10.1016/j.talanta.2007.10.051.
22. Ohno, T., Muramatsu, Y., Toyama, C., Nakano, K., Kakuta, S., and Matsuzaki, H. (2013). Determination of 129I in Fukushima Soil Samples by ICP-MS with an Octopole Reaction System. Anal. Sci. *29*, 271–274. https://doi.org/10.2116/analsci.29.271.
23. Ohno, T., Muramatsu, Y., Shikamori, Y., Toyama, C., Okabe, N., and Matsuzaki, H. (2013). Determination of ultratrace 129I in soil samples by Triple Quadrupole ICP-MS and its application to Fukushima soil samples. J. Anal. At. Spectrom. *28*, 1283–1287. https://doi.org/10.1039/c3ja50121c.
24. Muramatsu, Y., and Yoshida, S. (1995). Determination of I-129 and I-127 in Environmental-Samples by Neutron-Activation Analysis (Naa) and Inductively-Coupled Plasma-Mass Spectrometry (Icp-Ms). J Radioan Nucl Ch Ar *197*, 149–159. https://doi.org/10.1007/Bf02040227.
25. Matsueda, M., Aoki, J., Koarai, K., Terashima, M., and Takagai, Y. (2022). Mass-spectrometric determination of iodine-129 using O-CO mixed-gas reaction in inductively coupled plasma tandem quadrupole mass spectrometry. Anal. Sci. *38*, 1371–1376. https://doi.org/10.1007/s44211-022-00180-w.
26. Kimmig, S.R., Thompson, C., Baum, S., and Brown, C.F. (2021). Evaluation of iodine speciation and 129I/127I ratios at low concentrations in environmental samples using IC-ICP-MS. J Radioanal Nucl Ch *327*, 929–937. https://doi.org/10.1007/s10967-020-07537-3.
27. Kerl, W., Becker, J.S., Dietze, H.J., and Dannecker, W. (1996). Determination of iodine using a special sample introduction system coupled to a double-focusing sector field inductively coupled plasma mass spectrometer. J Anal Atom Spectrom *11*, 723–726. https://doi.org/10.1039/ja9961100723.
28. Kameo, Y., Ishimori, K.i., Shimada, A., and Takahashi, K. (2012). Simple Determination Method Using ICP-MS for 129I in Radioactive Liquid Waste Solidified with Bitumen. Bunseki Kagaku *61*, 845–849. https://doi.org/10.2116/bunsekikagaku.61.845.
29. Izmer, A.V., Boulyga, S.F., Zoriy, M.V., and Becker, J.S. (2004). Improvement of the detection limit for determination of 129I in sediments by quadrupole inductively coupled plasma mass spectrometer with collision cell. J. Anal. At. Spectrom. *19*, 1278–1280. https://doi.org/10.1039/b406478j.
30. Izmer, A.V., Boulyga, S.F., and Becker, J.S. (2003). Determination of 129I/127I isotope ratios in liquid solutions and environmental soil samples by ICP-MS with hexapole collision cell. J. Anal. At. Spectrom. *18*, 1339–1345. https://doi.org/10.1039/b306446h.
31. Hsieh, Y.K., Wang, T., Jian, L.W., Chen, W.H., Tsai, T.L., and Wang, C.F. (2014). An improved analytical method for iodine-129 determination in low-level radioactive waste. Radiochim. Acta *102*, 1137–1142. https://doi.org/10.1515/ract-2013-2161.
32. Grinberg, P., and Sturgeon, R.E. (2009). Ultra-trace determination of iodine in sediments and biological material using UV photochemical generation-inductively coupled plasma mass spectrometry. Spectrochim. Acta B *64*, 235–241. https://doi.org/10.1016/j.sab.2009.01.013.
33. Fujiwara, H., Kawabata, K., Suzuki, J., and Shikino, O. (2011). Determination of 129I in soil samples by DRC-ICP-MS. J. Anal. At. Spectrom. *26*, 2528–2533. https://doi.org/10.1039/c1ja10191a.
34. Farmer, O.T., Barinaga, C.J., and Koppenaal, D.W. (1998). Determination of 129I in ambient air by inductively coupled plasma mass spectrometry (ICP/MS). J Radioanal Nucl Ch *234*, 153–158. https://doi.org/10.1007/Bf02389764.
35. Ezerinskis, Z., Spolaor, A., Kirchgeorg, T., Cozzi, G., Vallelonga, P., Kjær, H.A., Sapolaite, J., Barbante, C., and Druteikiene, R. (2014). Determination of 129I in Arctic snow by a novel analytical approach using IC-ICP-SFMS. J Anal Atom Spectrom *29*, 1827–1834. https://doi.org/10.1039/c4ja00179f.
36. Cox, R.J., Pickford, C.J., and Thompson, M. (1992). Determination of I-129 in Vegetable Samples by Inductively Coupled Plasma Mass-Spectrometry. J. Anal. At. Spectrom. *7*, 635–640. https://doi.org/10.1039/ja9920700635.
37. Coralie, C., Azza, H., Michelle, A., Celine, A., Didier, B., Denis, M., and Lucilla, B. (2022). Mass-shift mode to quantify low level ^{129}I in environmental samples by ICP-MS/MS. J. Anal. At. Spectrom. *37*, 1309–1317. https://doi.org/10.1039/d2ja00128d.
38. Chang, F.C., Chao, J.H., and Tien, N.C. (2022). Determination of 129I activities and interference in low level radioactive waste by alkaline fusion coupled with ICP-MS. J Radioanal Nucl Ch *331*, 2029–2036. https://doi.org/10.1007/s10967-022-08252-x.
39. Brown, C.F., Geiszler, K.N., and Vickerman, T.S. (2005). Extraction and quantitative analysis of iodine in solid and solution matrixes. Anal. Chem. *77*, 7062–7066. https://doi.org/10.1021/ac050972v.
40. Brown, C.F., Geiszler, K.N., and Lindberg, M.J. (2007). Analysis of 129I in groundwater samples: Direct and quantitative results below the drinking water standard. Appl. Geochem. *22*, 648–655. https://doi.org/10.1016/j.apgeochem.2006.12.010.
41. Beals, D.M., and Hayes, D.W. (1995). Technetium-99, iodine-129 and tritium in the waters of the Savannah River Site. Sci. Total Environ. *173–174*, 101–115. https://doi.org/10.1016/0048-9697(95)04769-7.
42. Bandura, D.R., Baranov, V.I., and Tanner, S.D. (2002). Inductively coupled plasma mass spectrometer with axial field in a quadrupole reaction cell. J Am Soc Mass Spectr *13*, 1176–1185. https://doi.org/10.1016/S1044-0305(02)00435-X.
43. Adams, K.A., Morrison, S.S., Cherkasov, D.E., and Wall, N.A. (2021). Direct quantification of iodine in nuclear wastes using DRC-ICP-MS. J Radioanal Nucl Ch *328*, 491. https://doi.org/10.1007/s10967-020-07240-3.
44. Agilent-Technologies (2012). Agilent 8800 Triple Quadrupole ICP-MS: Understanding oxygen reaction mode in ICP-MS/MS. 2012, 5991-591708EN. https://www.agilent.com/cs/library/technicaloverviews/public/5991-1708EN_TechOverview_ICP-MS_8800_ORS_mode.pdf.
45. Zhu, Y. (2024). On-line generated ozone as a reactive cell gas for tandem quadrupole inductively coupled plasma mass spectrometry. Chem. Commun. *60*, 3974–3977. https://doi.org/10.1039/d4cc00636d.
46. De Laeter, J.R., Böhlke, J.K., De Bièvre, P., Hidaka, H., Peiser, H.S., Rosman, K.J.R., and Taylor, P.D.P. (2003). Atomic weights of the elements:: Review 2000 -: (IUPAC technical report). Pure Appl. Chem. *75*, 683–800. https://doi.org/10.1351/pac200375060683.
47. WHO (2022). Guidelines for Drinking-Water Quality: Fourth Edition Incorporating the First and Second Addenda (Whorld Health Organization).

STAR★METHODS

KEY RESOURCES TABLE

REAGENT or RESOURCE	SOURCE	IDENTIFIER
Chemicals		
Ammonium iodide	FUJIFILM Wako Pure Chemical Corp.	CAS: 12027-06-4
Radionuclide I-129	Eckert & Ziegler Analytics, Inc.	SN: 123794
Tetramethyl ammonium hydroxide	Tama Chemicals Corp.	CAS: 75-59-2
Instruments		
ICP-QMS/QMS	Agilent Technologies	Model: Agilent 8800
Ozone generator	EcoDesign Inc.	Model: LOG-LC15G
Ozone decomposer	EcoDesing Inc.	Model: ED-MD9-500s

EXPERIMENTAL MODEL AND STUDY PARTICIPANT DETAILS

It is not applicable to this study.

METHOD DETAILS

Wako special grade ammonium iodide was used to prepare ^{127}I solutions. A radio isotope solution (^{129}I, 101.9 Bq/g in 2% TMAH, traceable to the National Institute of Standards and Technology) was used to prepare ^{129}I solutions. TAMAPURE-AA grade TMAH solution (25%) and Ultrapur grade HNO_3 (60%) were used to prepare solutions for iodine analysis and multielement analysis, respectively.

The experimental system used in this study is illustrated in Figure S1. All the instruments (1–3), switching valves (made of perfluoroalkoxy alkanes (PFA)), connectors (made of PFA), and mass flow controllers (O_2, 2 L/min) are commercially available. Tubes connecting the instruments are made of PFA with an inner diameter of 1.0 mm and outer diameter of 3.0 mm. The mass flow controller is used to control the total flow rate of O_2 supplied to the ozone generator (1). This mass flow controller is set at the downstream of the ICP-QMS/QMS (3) to maintain the gas pressure supplied to the reaction cell. The ozone decomposer (2) at the upper stream of mass flow controller protects it from corrosion by ozone. Details with respect to the operating conditions are presented in the supplemental information.

Typical operating conditions for ICP-QMS/QMS were optimized for three sets of cell gas conditions: O_3 only, O_3 and H_2, O_3 and He, respectively. A preliminary optimization of the instrumental conditions was carried out with a well-used tuning solution (Li, Co, Y, Ce, and Tl, 1.0 ng/mL each in 2% HNO_3). The final optimization prior to analysis of iodine was carried out with a test solution (10 μg/mL of ^{127}I and 1.0 ng/mL and ^{129}I in 2% TMAH). The representative parameters are as follows: radio frequency power, 1500 W; sampling depth, 8.0 mm from the load coil; plasma gas flow rate, 14.0 L/min argon; carrier gas flow rate, 0.80 L/min argon; makeup gas flow rate, 0.45 L/min argon; extraction I lens, −1.8 V, 2.2 V, and −1.9 V for O_3 reaction, O_3 and H_2 reaction, and O_3 and He reaction, respectively; extraction 2 lens, −205 V, −130 V, and −225 V for O_3 reaction, O_3 and H_2 reaction, and O_3 and He reaction, respectively; omega bias lens, −165 V, −165 V, and −185 V for O_3 reaction, O_3 and H_2 reaction, and O_3 and He reaction, respectively; omega lens, 23.5 V, 23.6 V, and 25.7 V for O_3 reaction, O_3 and H_2 reaction, and O_3 and He reaction, respectively; cell gas flow rate, 0.3 mL/min O_3, 0.3 mL/min O_3 with 10 mL/min H_2, and 0.3 mL/min O_3 with 10 mL/min He, respectively; octopole reaction cell inlet, −50 V; octopole reaction cell outlet, −70 V; octopole bias, −5.0 V; deflecting lens, 3.8 V, 0.6 V, and 1.2 V for O_3 reaction, O_3 and H_2 reaction, and O_3 and He reaction, respectively; energy discrimination, −7.0 V; integration time, 0.1 s for ^{127}I related ions, 5.0 s for ^{129}I related ions, 1.0 s for other ions.

QUANTIFICATION AND STATISTICAL ANALYSIS

A mixed solution of Sb and Ba, 100 ng/mL each in 2% HNO_3, was measured for correction of mass discrimination. The measured ion pairs were $^{121}Sb^+ \rightarrow {}^{121}Sb^{16}O^+$, $^{123}Sb^+ \rightarrow {}^{123}Sb^{16}O^+$, $^{121}Sb^+ \rightarrow {}^{121}Sb^{16}O_2^+$, $^{123}Sb^+ \rightarrow {}^{123}Sb^{16}O_2^+$, $^{135}Ba^+ \rightarrow {}^{135}Ba^{16}O^+$, $^{137}Ba^+ \rightarrow {}^{137}Ba^{16}O^+$, $^{135}Ba^+ \rightarrow {}^{135}Ba^{16}O_2^+$, and $^{137}Ba^+ \rightarrow {}^{137}Ba^{16}O_2^+$, respectively. For example, the correction factor obtained with measurement of $Sb^+ \rightarrow SbO^+$ can be expressed as: $F_{Sb} = R_{Sb}{}^*/R_{Sb}{}^0$, where R is the signal intensity ratio of ($^{123}Sb^+ \rightarrow {}^{123}Sb^{16}O^+$)/($^{121}Sb^+ \rightarrow {}^{121}Sb^{16}O^+$), $R_{Sb}{}^*$ and $R_{Sb}{}^0$ denoting the real ratio and the observed ratio, respectively. For the measurement of $I^+ \rightarrow IO^+$, the real ratio $R_I{}^*$ can be calculated from the observed ratio $R_I{}^0$ as: $R_I{}^* = R_I{}^0 \times (0.57 \times F_{Sb} + 0.43 \times F_{Ba})$, where 0.57 and 0.43 were the weight parameters considering the differences between isotopic masses of ^{121}Sb-to-^{127}I and ^{127}I-to-^{135}Ba, respectively.

Following the instruction of the manual of the ICP-QMS/QMS instrument, dead-time correction was conducted for signal intensities exceeding 1,000,000 CPS. The equation for dead-time correction was $S^* = S^0(1\text{-}S^0 \times t)$, where S^*, S^0, and t denote the signal intensity after correction, the initial signal intensity, and dead-time of the detector (30 ns for the present instrument), respectively.

Statistical analysis for calculations of mean values and their standard deviations were conducted with Excel for Microsoft 365. The value following "mean value ±" shows the standard deviation obtained from 10 repetitions of measurement, i.e., $n = 10$.

ADDITIONAL RESOURCES

All electronic structure calculations were performed using the Gaussian 16 suite. The energies of the atomic cations were obtained by ωB97XD hybrid functional and the split valence triple zeta basis set, Def2TZVP. The optimized geometries of the complexes of atomic cation and oxygen atoms were obtained via optimization using the ωB97XD/Def2TZVP level of theory. The obtained geometries were then characterized by frequency calculations to determine the zero-point vibrational energy. To establish the energetics required for the reaction, the transition state geometries were optimized at the ωB97XD/Def2TZVP level and confirmed by verifying the existence of an imaginary part of their vibrational frequencies. The connections between the transition states, reactants, and products were examined using an intrinsic reaction coordinate analysis, starting from the transition state geometry. The harmonic frequencies obtained by frequency analysis were used to determine the zero-point energy corrections.